HAL open science

Evaluating the impact of urban morphology on rooftop solar radiation: A new city-scale approach based on Geneva GIS data

Alessia Boccalatte, Martin Thebault, Christophe Ménézo, Julien Ramousse, Marco Fossa

To cite this version:

Alessia Boccalatte, Martin Thebault, Christophe Ménézo, Julien Ramousse, Marco Fossa. Evaluating the impact of urban morphology on rooftop solar radiation: A new city-scale approach based on Geneva GIS data. Energy and Buildings, 2022, 260, 10.1016/j.enbuild.2022.111919 . hal-03703326

HAL Id: hal-03703326

https://hal.science/hal-03703326

Submitted on 31 May 2023

HAL is a multi-disciplinary open access archive for the deposit and dissemination of scientific research documents, whether they are published or not. The documents may come from teaching and research institutions in France or abroad, or from public or private research centers.

L'archive ouverte pluridisciplinaire **HAL**, est destinée au dépôt et à la diffusion de documents scientifiques de niveau recherche, publiés ou non, émanant des établissements d'enseignement et de recherche français ou étrangers, des laboratoires publics ou privés.

Highlights

- A new approach is developed for large scale urban morphological studies
- The Canton of Geneva (60,000 buildings) is selected as a case study
- 40 morphological features are investigated towards rooftop insolation
- Moderate Pearson coefficients (R^2=0.2/0.4) are found for the whole dataset
- Densest municipalities exhibit higher correlation levels (R^2=0.4/0.6)

Graphical Abstract

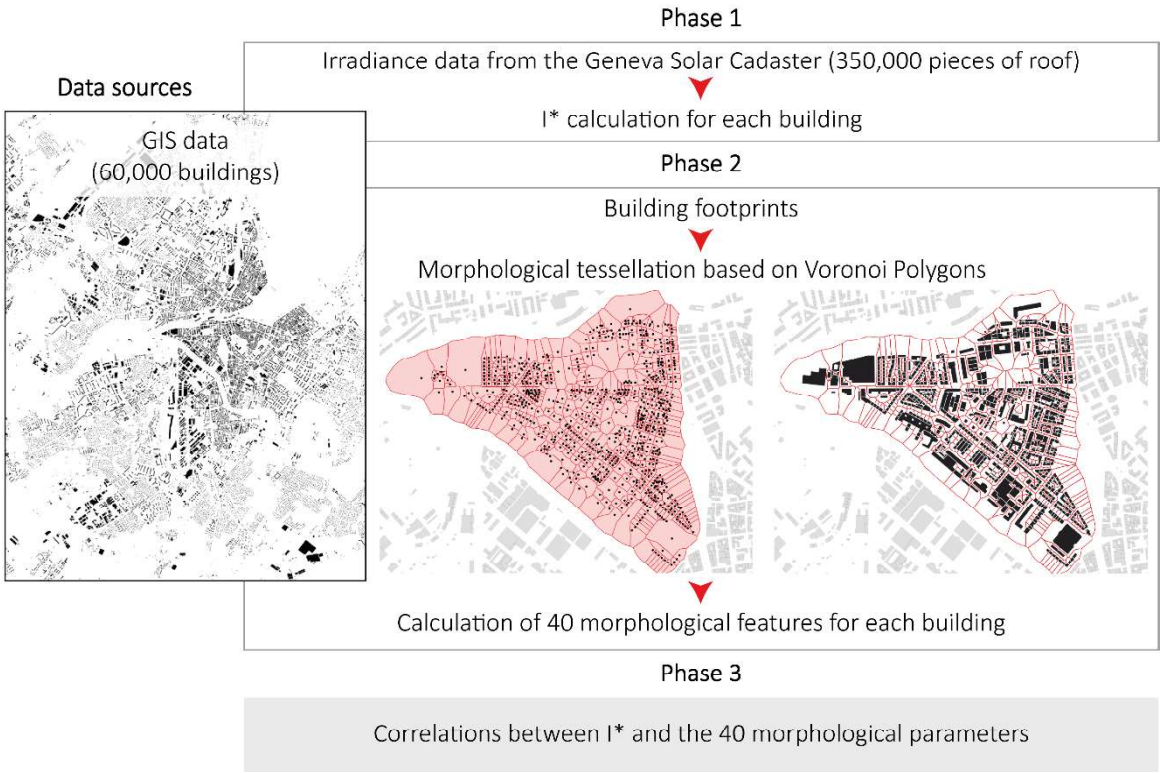

Manuscript File Click here to view linked References

Evaluating the impact of urban morphology on rooftop solar radiation: a new city-scale approach based on Geneva GIS data

Alessia Boccalatte[a,b], Martin Thebault[a], Christophe Ménézo[a], Julien Ramousse[a], Marco Fossa[b]

[a] LOCIE UMR CNRS 5271 - Polytech'Annecy-Chambéry, France
[b] DIME - Department of Mechanical, Energy, Management and Transportation Engineering, University of Genova, Italy

*Corresponding author e-mail: alessia.boccalatte@univ-smb.fr

Abstract. Building rooftops represent one of the most valuable resources to harvest solar energy in cities. Nevertheless, this potential is limited by the urban morphology impacting the shading conditions. This study suggests a general methodology to assess the impact of urban form on solar harvesting. To this aim, a new GIS-based approach is developed to extract meaningful morphological parameters at a very large scale. The rooftop overall shading rate is here defined as a benchmark, and it is measured through a scaled insolation representing the ratio between the insolation of a surface within the urban context and its unshaded theoretical maximum. A set of 40 morphological features is calculated for 60,000 buildings in the Canton of Geneva (Switzerland), and the scaled solar insolation of about 350,000 roof pieces is derived from the Solar Cadaster of Geneva. The results outline the insolation distribution within the city and as a function of urban morphology. The rooftop overall shading rate shows moderate Pearson coefficients (r=0.2/0.4) towards some parameters, namely building height, volume, and height difference with surroundings, while others seem irrelevant. Analysing the 48 Geneva municipalities one at a time, the denser downtown areas reach higher correlation levels (r=0.4/0.6) compared to the suburban ones.

Keywords: *Urban Morphology; Rooftop Solar Radiation; Solar Cadaster; GIS; Correlation Analysis*

1 Introduction

The decrease of building energy consumption and the exploitation of renewable resources are key goals of the current EU regulation toward energy transition in urban areas [1]. In Europe, the buildings and the building construction sector combined account for 35% of the total global final energy consumption but new constructions are expected to reduce considerably their energy use thanks to the more stringent policies [2]. However, if we take into account the growth of the world's population, urbanization and the low rate of renewal of the building stock (less than 1% per year), efforts have to be accentuated and ensure that buildings also produce energy. The relatively recent concept of Nearly Zero Energy Buildings (NZEB) and Districts (NZED), has helped to develop more awareness on on-site energy production issues [3,4]. In this context, solar energy stands out among renewable sources for its ease of adaptation to urban surfaces. Based on the International Energy Agency (IEA) projections more than 50% of the overall photovoltaic capacity will be installed on residential and commercial buildings by 2050 [5]. Thus, cities play a central role to boost renewable energy production at a larger scale than standalone building or district installations.

The solar resource varies to a great extent with the time scale and location, and efficient exploitation requires a high level of knowledge on the actual resource. In the last decades, thanks to the great improvement in large scale simulation, open-source geographic datasets, and Light Detection and Ranging (LiDAR) data acquisition, it has been possible to assess the solar energy potential of a city at

a macroscale, resulting in a solar map or solar cadaster [6]. However, as it emerges from the study by Kanters et al. [7], there is still a restricted number of accurate city-scale solar cadasters. These solar cadasters give access to an average annual irradiation on the roofs or even an average annual energy production depending on the solar technology selected. Nevertheless, the main limiting factors are the complex shadowing conditions and building radiation interreflections [8] having an impact on computation time, and the high level of expertise required to set up radiation models and large scale simulations. Given the difficulty of computing the solar potential at an urban territory scale, another key issue regarding the distribution of solar radiation within the urban environment is to analyse the effects of the urban form, or morphology, on solar availability. This could contribute to create guidelines for urban planners at the early design stage and help municipalities to identify the most suitable areas to harvest solar energy.

In the last decade, there has been a significant interest in investigating the effect of the urban form on both building energy performance [9–12] and solar power potential analyses [13–17]. Some parametric studies on elementary and ideal urban archetypes evidence strong correlations between morphological features and irradiance levels [18]. Despite being a very useful reference for designers and planners, this level of accuracy in the results cannot be expected when dealing with real and highly heterogeneous systems such as real cities. In the last few years, also thanks to the growing availability of 3D (or 2.5D) information about cities, there has been significant progress in managing real urban data. Chatzipoulka et al. [19] investigated the relationship between urban geometry and solar availability on building façades and open spaces of 24 neighbourhoods of London of the size of 500 m x 500 m. Mohajeri et al. [20] studied the effects of 6 relevant urban compactness indicators on the solar potential of 16 districts (11,418 buildings) of the city of Geneva (Switzerland). Also, Morganti et al. [21] evaluated the impact of 7 morphological features on the façade solar irradiance of 14 urban textures of Rome (Italy) and Barcelona (Spain). While these studies outline the relationship between solar potential and the urban texture, they are mostly focused on façades and the calculation of the morphological features is generally done at the neighbourhood level, averaging the building characteristics within a certain administrative border or cell of a squared grid. Additionally, the considered sample of buildings is often limited to a few thousand and the selection of the morphological features does not follow a rigorous methodology, being considerably variable depending on the research objectives.

In the meantime, substantial advances have been done in the so-called Urban Morphometrics (UMM) [22–24], a branch of urban morphology study aiming at developing objective and reproducible methodologies to compute rigorously the geometrical attributes of a city to support scientific researches. In particular, Fleischmann et al. [25–28] developed a new approach to derive a meaningful spatial unit of analysis at the building scale (in other words the “surface of influence” of a building), allowing the calculation of several morphological attributes related to the buildings themselves and the adjacent surroundings. This process has been also implemented in a python library called Momepy [29], thus enabling automatization and reproducibility.

The present study is intended to fill three main research gaps. Firstly, despite the recent improvements in solar cadasters, a lack of statistical analyses related to the solar radiation distribution within the urban context can be highlighted. These studies mainly concern the solar radiation model and computational issues, without any interpretation of the results with a view to urban morphology. Secondly, it has been pointed out the necessity to establish a systematic in-depth analysis to assess meaningful morphological features at the building scale and to investigate the correlations with insolation without averaging the urban characters. Finally, the use of very large building datasets seems to be still very restricted.

The present research is related to calculating and analysing 40 morphological features (including building geometry, shape, density, spatial distribution) on each of the 60,000 buildings of the Canton of Geneva through GIS data and the Momepy library [29]. The yearly rooftop insolation data from the Solar Cadaster of Geneva [30,31] have been analysed in relation to urban morphology. Finally, Pearson correlation analysis has been performed without averaging the features at the neighbourhood level. The results provide interesting statistical findings regarding the potentially most influential

parameters for solar urban planning, but also the city-related morphological specificities and their impact on solar harvesting.

2 Data and methods

The following sections include an outline of the data sources and methods. The methodology is schematically represented in Figure 1Figure 1. The workflow highlights the three main phases of the developed approach, i. e. the computation of the scaled solar insolation (I*, as defined in Eq.9) derived by the Solar Cadaster of Geneva, the morphological tessellation and the consequent calculation of the 40 selected parameters for each building, and finally the analysis of the results arising from the statistical correlations.

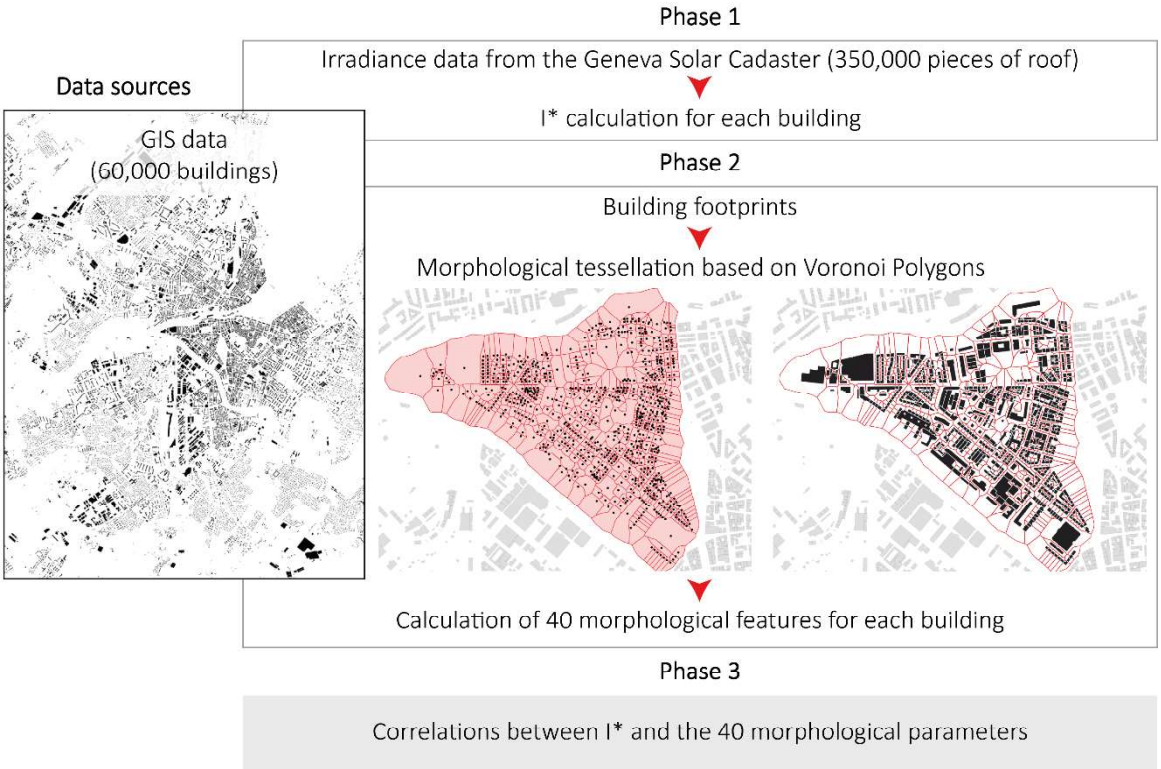

Figure 1: Schematic representation of the developed methodology shown in a specific area of the Canton of Geneva.

2.1 GIS data sources and case study

The present paper proposes a general methodology to evaluate the impact of urban morphology on the rooftop solar potential for large city-scale studies. Worth noting, the developed approach is general and it applies to any urban area and considering any benchmark in addition to rooftop insolation.

This methodology is then applied to a case study: the Canton of Geneva (46° 13′ 05″ N, 6° 09′ 58″ E, Switzerland). Its total surface is 282 km^2 and it comprises about 60,000 buildings subdivided into 48 municipalities.

The input data to the present GIS-based analysis comprise building geometry and solar radiation information in the form of geospatial vector data for Geographic Information Systems. One of the most common format to handle vector data is the shapefile, which stores a set of georeferenced attributes for each element (here the buildings), depending on the information needed. This study involves two shapefiles retrieved from the on-line repository of the Geneva territory (SITG: *Le système d'information du territoire à Genève*) [32], namely *Cad.batiment.hors.sol* and *Ocen.solaire.irr.surface.utile*. The first gathers general information about the building, such as period of construction, belonging municipality, final use and, most important here, the building height. The

second concerns solar radiation and geometrical information (slope and azimuth) of each piece of roof. Figure 2 shows the two shapefiles within the QGIS environment with a non-exhaustive attribute table of the most important information stored in each. The colour scale of *Ocen.solaire.irr.surface.utile* refers to the yearly average solar insolation (kWh/m^2 year) received by each piece of the rooftop as computed in [30,31] to build the Solar Cadaster of Geneva. One can note that the size of the two shapefiles is different: *Cad.batiment.hors.sol* stores a set of information for each building (about 60,000 elements), whereas *Ocen.solaire.irr.surface.utile* is related to each piece of roof (about 350,000 elements).

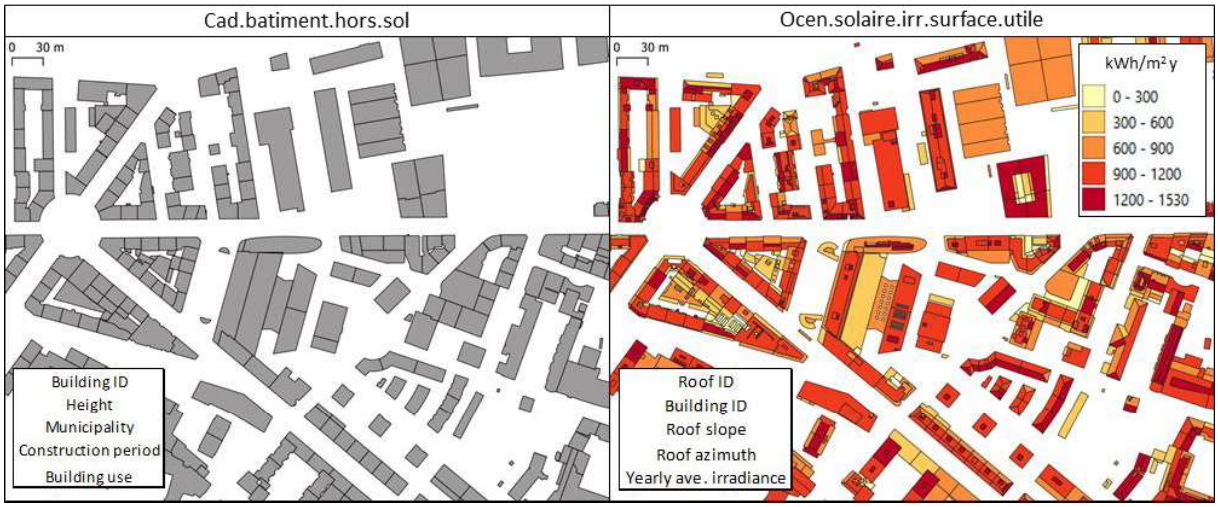

Figure 2: Insight of the two shapefiles, Cad.batiment.hors.sol and Ocen.solaire.irr.surface.utile, and the related main attributes. Zoom on a specific area of Geneva.

3 Definition of I, the scaled solar insolation*

As briefly outlined in the Introduction section, the key issue of the developed approach relates to the investigation of the relationship between the building rooftop overall shading rate and the morphological parameters. A scaled solar insolation (I*) has been introduced as a measure of the shading level of a building rooftop. I* has been defined as the ratio between the insolation of a roof surface within the urban context and its unshaded theoretical maximum, as a function of its slope (β) and azimuth (γ). I* is a dimensionless parameter, ranging from 0 to 1, which represents the share of theoretical maximum insolation (without any shading) that can be attained by a rooftop surface within the urban context. The closer I* gets to 1, the lower is the building rooftop overall shading rate, approaching the unshaded condition.

For the calculation of I*, the yearly average solar insolation (in kWh/m^2 year) received by each piece of rooftop (about 350,000 elements) within the Canton of Geneva has been retrieved from the open-access Geneva Geoportail (SITG) [32] in the Energy section (shapefile *Ocen.solaire.irr.surface.utile*). The city-scale insolation computation was carried out in the framework of the development of the Solar Cadaster of Geneva [30,31,33]. The latter is a powerful integrated tool involving the use of LiDAR, 2D and 3D cadastral data. The solar radiation modelling was implemented through GIS in combination with Matlab, using the Hay anisotropic model for sky-diffuse radiation [34] and accounting for the shading coefficients on the direct and diffuse components [35].

For each piece of rooftop (i), having a certain slope (β) and azimuth (γ), the dimensionless scaled solar insolation (I^*_{roof}) has been calculated as in Eq.999999

$$I^*_{roof}(i) = \frac{I_{roof}(i)}{I_{theo-max}(\beta,\gamma)} \quad (1)$$

where I_{roof} is the surface yearly average solar radiation (in kWh/m^2 year) of the ith surface extracted from the Solar Cadaster of Geneva and $I_{theo\text{-}max}$ is the unshaded theoretical maximum insolation that corresponds to the ith surface, calculated from its slope (β(i)) and azimuth (γ(i)). In other words, considering a specific piece of rooftop (i), $I_{theo-max}(\beta(i),\gamma(i))$ can be seen as the yearly solar radiation that would be received by this roof if it were not shaded by surroundings elements (buildings, elements on the roof etc). Therefore a I^*_{roof} value of 1 corresponds to a roof that is not shaded at all.

The calculation of $I_{theo\text{-}max}$ is based on the well-known plane-of-array (POA) solar radiation formulation, evaluating the incident insolation on a tilted surface (β, γ) from horizontal radiation data (transposition model) as in Eq.2

$$I_{theo-max}(\beta,\gamma) = I_{dir}(\beta,\gamma) + I_{diff}(\beta,\gamma) + I_{refl}(\beta) \tag{2}$$

where I_{dir}, I_{diff}, I_{refl} are respectively the direct, the diffuse, and the reflected solar radiation components. To be consistent with the calculations of the Solar Cadaster of Geneva, the Hay model has been chosen for diffuse radiation, and the same (with respect to the Cadaster) horizontal monthly average insolation data have been used as the input for the maximum unshaded insolation calculation. A heuristic approach has been adopted for further validation: $I_{theo\text{-}max}$ has been compared with the maximum insolation value ($I_{roof\text{-}max}$) extracted from the Cadaster for each possible combination of slope and azimuth (β, γ) as in Eq.3

$$I_{roof-max}(\beta,\gamma) = \max(I_{roof}(i), (\beta(i),\gamma(i)) = (\beta,\gamma)) \tag{3}$$

The main idea behind the calculation of $I_{roof-max}$ is that, considering the large number of roof surfaces in the dataset, it could be expected that, for each possible combination of slope and azimuth, there is at least one roof that should be unshaded so that $I_{roof-max}(\beta,\gamma) = I_{theo-max}(\beta,\gamma)$.

The relative error (Δ) between the two quantities is calculated in percentage as in Eq.4

$$\Delta(\beta,\gamma) = \left(\frac{I_{theo-max}(\beta,\gamma) - I_{roof-max}(\beta,\gamma)}{I_{theo-max}(\beta,\gamma)}\right)\cdot 100 \tag{4}$$

Worth noting, to be consistent with the abovementioned assumption, $I_{roof\text{-}max}$ can be compared to the unshaded condition ($I_{theo\text{-}max}$) only when the number of surfaces (having the same slope and azimuth values) is sufficient to assume that at least one among them is not shaded. This condition is not always met, typically when β>40°, since highly inclined roof surfaces are less common and more likely to be shaded from surroundings. Here, the minimum number of roof surfaces that is considered statistically significant, and thus allowing the calculation of the error Δ, is set to 30. Despite the heuristic validation has been carried out for a reduced dataset, being the calculation of $I_{theo\text{-}max}$ identical for all the surfaces, the validation process can be extended to the whole dataset. Figure 3 shows the values of $I_{theo\text{-}max}$ (left), $I_{roof\text{-}max}$ (centre), and Δ (right), as a function of the surface slope (β) and azimuth (γ). It can be observed that the general appearance of $I_{theo\text{-}max}$ and $I_{roof\text{-}max}$ is very similar, with some punctual differences and a greater disagreement for β>40° due to the scarcity (less than 30) of comparable surfaces. The mean Δ is 3.26%, with some localized peaks of 10%, which is considered acceptable. As expected, Δ is mostly positive meaning that $I_{theo\text{-}max}$ is generally higher than $I_{roof\text{-}max}$ due to the not-perfect unshaded conditions within the urban environment (despite the limitation set to 30 buildings).

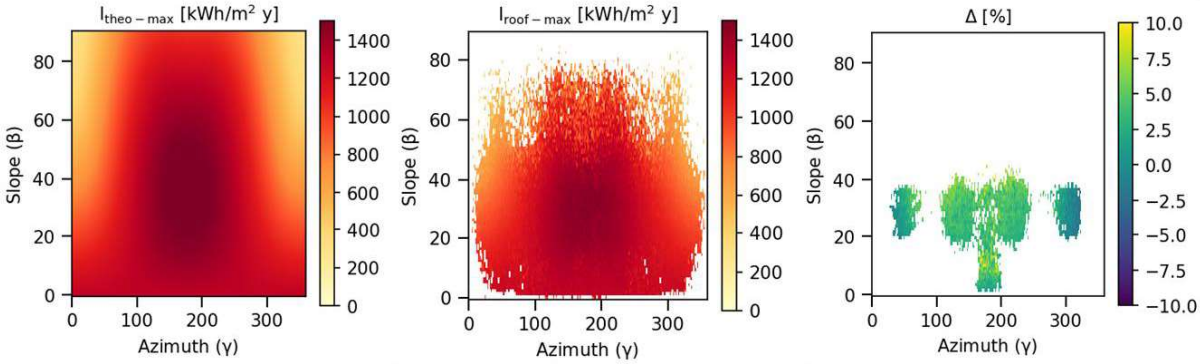

Figure 3: $I_{theo\text{-}max}$ (left), $I_{roof\text{-}max}$ (centre), and the relative error Δ (right) as a function of the surface slope (β) and azimuth (γ)

Since the evaluation of the morphological parameters is made for each building and not for each roof, I^*_{bld} is introduced. It corresponds to the average area-weighted value of I^*_{roof} for each building and it is calculated as in Eq.5:

$$I^*_{bld} = \frac{\sum_{i \in bld} I^*_{roof}(i) \cdot A_{roof}(i)}{\sum_{i \in bld} A_{roof}(i)} \tag{5}$$

where A_{roof} is the area of each roof surface. As all the following analyses are related to the building elements, from now on, I^*_{bld} will be simply denoted as I* for the sake of brevity. At this point it is worth mentioning that the proposed methodology is perfectly suitable for the study of insolation received by façades. However, this information is still not available yet at the scale of the Canton of Geneva.

4 Morphological tessellation and calculation of urban form features

This study aims at evaluating the relationship between the building rooftop overall shading rate, measured through I*, and the characteristics of the urban environment. A set of 40 meaningful morphological features have been selected and calculated for each building of the Canton of Geneva. Differently from previous studies [19–21], where the urban morphological parameters were related to average values within a predefined reference boundary (grid or municipality), here the objective is to obtain a non-averaged unique value for each building. Indeed, meaningful indicators should capture not only simple geometrical attributes of one building (namely the height, surface, volume, …) but also its relationship with the surroundings (namely the inter-building distance, density, height difference with neighbours, and more).

From the 60,000 building footprints and the building height information stored in the shapefile *Cad.batiment.hors.sol*, a python script has been implemented to extract the selected urban metrics. To this aim, a package named Momepy [29] has been exploited. The Momepy library is based on the other hand on well-known python packages for GIS data analysis as GeoPandas [36], PySAL [37], and networkX [38]. It provides several algorithms measuring six categories of features: *dimension*, *shape*, *intensity*, *spatial distribution*, *connectivity*, and *diversity*, identified by the developers through detailed literature research [25]. In the present study, 40 among the attributes measuring building *dimension*, *shape*, *intensity*, and *spatial distribution* have been selected. The list of features, as well as the related equations and description, is reported in the Appendix for the sake of conciseness. The categories of *connectivity* and *diversity* (as defined in [29]) are not included in this research as they are mainly related to network analysis and they are not representative for solar studies related to the resource spatial distribution.

The *dimension* category concerns the basic geometrical attributes of a building (perimeter, footprint and total floor areas, volume, longest axis length, and more), whereas the *shape* group includes some shape descriptors (e. g. degree of elongation, compactness, squareness, shape index). Contrarily to the previous categories, which are strictly related to the building geometry, the *intensity* category is more

related to the urban fabric, comprising the calculation of the density. In urban studies, density is generally defined as the ratio between the footprint area (or the total floor area) and the unbuilt space. The calculation of the density requires the definition of a reference boundary that is often established using a grid or by simply considering the administrative limits of a district. However, this approach results in averaged values of a space portion, and it fails in capturing site-specific and building-related density information. To overcome this limitation, the Momepy *morphological tessellation* function is used to evaluate the "surface of influence" of each building. The tessellation cell is a geometric derivative of Voronoi polygons obtained from building footprints. It represents the smallest spatial unit that delineates the portion of land around each building. Through the morphological tessellation, it is thus possible to capture the influence that each building exerts on the surrounding space as well as the building-related density information. Figure 4 shows the building footprints and the space subdivision into tessellation cells in a selected portion of the city of Geneva. The colour scale shows the *intensity* of the built environment in terms of building Coverage Area Ratio (CAR) expressed as the ratio between the building footprint area and the area of the related tessellation cell. As it can be observed from the figure, the darker is the colour the greater is the proportion of the tessellation cell covered by the building footprint, thus mapping precisely the densest areas within the urban fabric.

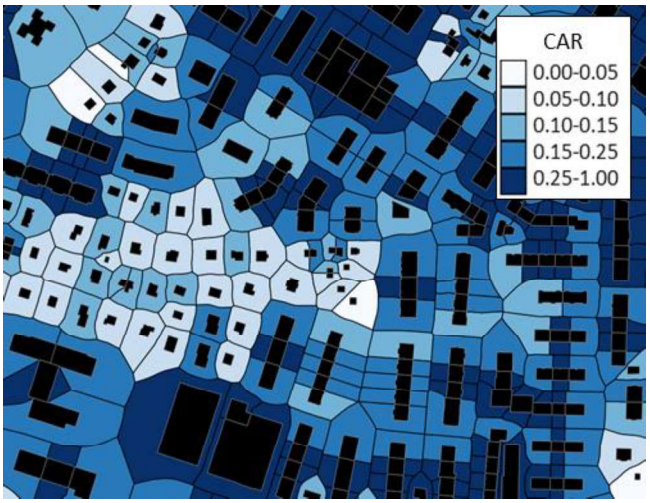

Figure 4: Building footprints and related tessellation cells of a specific area of Geneva. The colour scale is related to the building Coverage Area Ratio (CAR)

The *spatial distribution* aims at capturing the spatial relationships among buildings. Each building is influenced by its surroundings and it must be analysed within a spatial context, accounting for the neighbouring elements. This is possible using the *spatial weights*, i. e. mathematical structures used to detect the relationship between elements in the form of a binary matrix (1 = neighbours, 0 = not neighbours). In a few words, a building neighbour is a building whose tessellation cell is adjacent to the one under consideration as it is schematically represented in Figure 5.

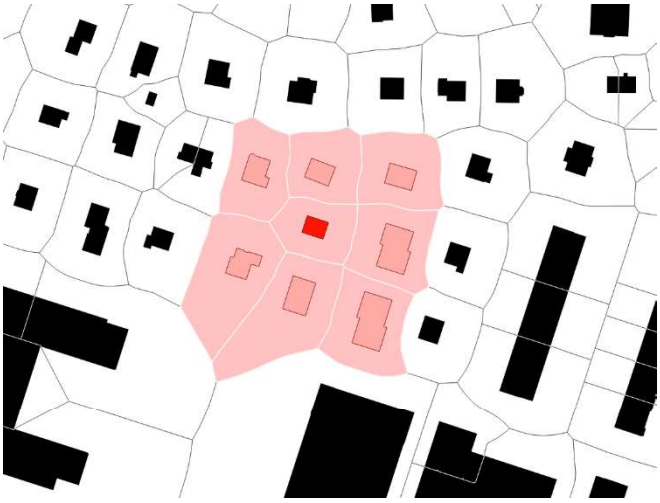

Figure 5: Schematics representation of a building (red) and its neighbours identified by the spatial weights

Once the neighbours are defined, some morphological features, such as the mean distance to neighbouring constructions or averaged characters of the surroundings (average building height, surface, volume, and many others on adjacent cells), have been calculated.
Finally, a set of additional morphological parameters that are not included in the Momepy library has been considered for this specific solar-related analysis. In more detail, the area-weighted average rooftop slope is calculated as in Eq.6

$$\bar{\beta} = \frac{\sum_{i \in bld} \beta_{roof}(i) \cdot A_{roof}(i)}{\sum_{i \in bld} A_{roof}(i)} \tag{6}$$

where $\beta_{roof,}$ and A_{roof} are respectively the slope and the area of each piece of roof (i).
The average Height to Width (HW) ratio, a useful measure for urban street canyon analyses, is evaluated through Eq.7

$$HW = \frac{1}{N_{neigh}} \sum_{j \in neigh} \frac{H}{d(j)} \tag{7}$$

77777
where H is the height of the reference building and the subscript 'neigh' refers here to the set of neighbouring buildings. N_{neigh} is the number of neighbours and d(j) is the distance between the reference building and its jth neighbour.
The distance-weighted average height difference ($\overline{\Delta H}$) has been also introduced as in Eq.8

$$\overline{\Delta H} = \frac{\sum_{j \in neigh} (H(j) - H) \cdot w(j)}{\sum_{j \in neigh} w(j)} \tag{8}$$

where H(j) is the height of the jth neighbour, and w(j) are the distance-weights for the average. Here, w(j) is the inverse of the distances between the reference building and its neighbours (w(j)=1/d(j)), thus giving more weight to the nearest constructions as they are expected to have a greater impact on solar potential. Likewise, also the positive distance-weighted average height difference ($\overline{\Delta H}^{+}$) is defined, including in the calculation only the neighbours that are higher than the building itself (H(j)> H).
Finally, the angle α, the average neighbourhood shading angle, is expressed through Eq.9

$$\alpha = \arctan\left(\frac{1}{N_{neigh}} \sum_{j \in neigh} \frac{H(j) - H}{d(j)}\right) \quad (9)$$

As for $\overline{\Delta H}$, the positive α (α^+) is also included considering only the neighbouring buildings that are higher than the considered one (H(j)> H).

5 *Data pre-processing*

A series of pre-processing operations have been performed to set up the statistical analysis and the correlations between I* and the morphological parameters (M_n, with n ranging from 1 to 40). First, missing values have been checked and removed. The building dataset has been cleaned from not significant elements, i. e. buildings having a footprint area below 20 m^2 and/or a height lower than 3 m, representing approximatively the 0.03% of the total elements. In addition, when investigating the correlations between I* and the morphological features, the outlier buildings, having height, footprint area or tessellation area values significantly higher than the rest of the dataset, have been removed using an Isolation Forest method implemented in a scikit-learn python package [39]. Finally, the data related to both the scaled insolation and the urban morphology have been merged using the building ID (named 'EGID' in the shapefiles) thus obtaining a table of attributes, composed by the 40 morphological features plus one value of I*, for each building.

6 *Results and discussion*

In the following sections, the results are presented. The first two parts are related to the statistical analysis on the distribution of I* (Section 6.1) and the morphological differences between the buildings with respectively the lowest and highest values of I* (Section 6.2). To this aim, two groups of buildings have been identified within the dataset through quantiles. The first one (Q_{10}) comprises all the buildings having a I* value lower than the 0.1 quantile, whereas the second (Q_{90}) is related to the ones with I* higher than the 0.9 quantile. The morphological features of Q_{10} (lowest I*) and Q_{90} (highest I*) have been analysed and compared interpreting boxplots.

Sections 6.3 and 6.4 investigate the correlations between I* and the morphological features. The Pearson Correlation coefficients (R^2) and the scatter plots between I* and each morphological feature (M_n) have been calculated and analysed to investigate the correlation between the dependent variable y (I*) and the independent variable x (M_n). In some cases, M_n resulted in a non-normal distribution and, to reduce the skewness of data and get a more linear relationship, different types of mathematical transformations on the original dataset have been tested. Following Stevens [40], the logarithmic and square-root transformations in some cases proved to be more effective to represent the relationship between I* and M_n. The correlation study has been carried out in the first instance on the whole building dataset (Section 6.3), and then within the different 48 municipalities of the Canton of Geneva evidencing the differences as a function of the urban characteristics (Section 6.4).

6.1 *I* distribution over the Canton of Geneva*

Figure 6 shows the histogram of the I* distribution over the 60,000 buildings. The I* values on the x-axis have been subdivided into 50 homogeneous intervals and the y-axis represents the related percentage of buildings with respect to the total number. As it can be observed, the I* distribution is characterized by a negative skewness, i.e. the mass of the distribution is concentrated on relatively high I* values.

It can be also noticed that buildings with an I* value of 1.0 are also infrequent. This mean that the urban morphology affects most of the time the building rooftop irradiance, either by affecting the whole building or by affecting one piece of roof of the building since I* is an average value (see Eq.5). Nevertheless, it is worth considering that there could be slight discrepancies between the calculation of $I_{theo\text{-}max}$ and the insolation values as computed by the Solar Cadaster of Geneva. Indeed, even if, in the present paper, same hypothesis regarding reflections and diffusion model were made, considering the complexity of the calculation, the results might be affected by some minor differences. However, even by considering an uncertainty of 10% (which corresponds to a rather conservative value of uncertainty

with regards to the validation conducted in Section 3) it appears that more than 75% of the buildings have a I* below 0.9 and can therefore be considered as partly shaded.

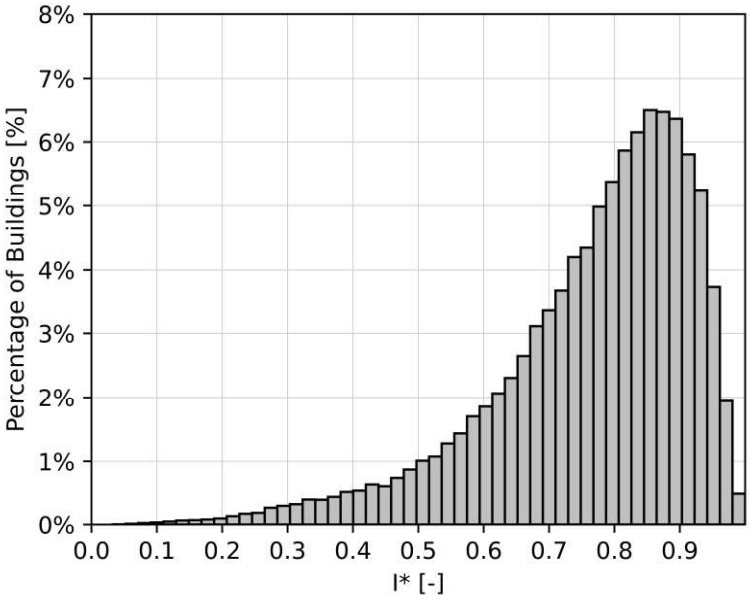

Figure 6: Distribution of I on buildings*

The related cumulative distribution function of I* is shown in Figure 7. The mean I* value is 0.77 and the 25th percentile is 0.69 meaning that in general, despite the overall influence of the urban morphology on the solar resource, the shading levels are quite low.

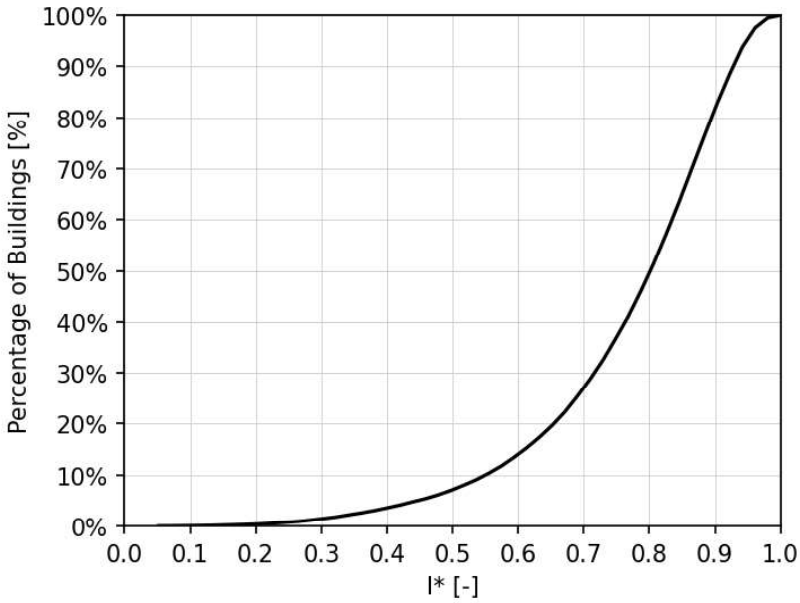

Figure 7: Cumulative distribution function of I on buildings*

6.2 Statistical analysis of the shading conditions as a function of the urban morphology

Figure 8 outlines a summary statistic (median and interquartile range) of the selected lower (Q_{10}) and the upper (Q_{90}) quantiles of I* with respect to the main meaningful morphological features, whose values are reported into the y-axis. In more detail, the size of the two groups is identical (both represent the 10% of the total number of buildings) but Q_{10} comprises all the buildings having an I* lower than 0.55, whereas Q_{90} includes the ones with an I* higher than 0.93. The analysis is aimed at

evidencing the main morphological differences between more shaded buildings (light blue, Q_{10}) and the less shaded ones (red, Q_{90}). Boxplots show the minimum (lower cap), maximum (upper cap), median (box middle line), 25th percentile (lower box limit), and 75th percentile (upper box limit) value of the selected morphological features for the two groups.

Concerning the height (H), the footprint area (A), and the total floor area (fA), the boxplots representing the group Q_{90} are comparatively higher than the ones that represent Q_{10}, meaning that taller and bigger (in terms of areas) constructions are more likely to be less shaded. The spread of the boxplots represents the variability of a parameter. Observing the total floor area (fA), the variability is much lower for Q_{10}, meaning that in general the rooftop shading mainly affects small constructions, with a fA typically lower than 250 m^2.

The boxplots of the Volume to Façade Ratio (VFR) evidence that Q_{90} mainly comprises constructions that have a big volume compared to the façade area. In other words, low-rise large buildings (with higher VFR) are generally less shaded than the high-rise/tower-like ones. In terms of urban density, if we refer to the building Floor Area Ratio (FAR), i. e. the ratio between the building total floor area and the area of the related tessellation cell, it is possible to notice higher density values for less shaded buildings (Q_{90}). This is apparently in contrast with previous studies that evidence a negative correlation between solar radiation and density. However, as highlighted in the Introduction, thanks to the tessellation, here the calculation of the FAR density is not averaged within a selected area, but it is computed within each tessellation cell, thus resulting in a building-related parameter independent from the characteristics of the surroundings.

Contrarily, referring to the urban density as the average Floor Area Ratio of neighbouring constructions ($\overline{FAR}$), lower $\overline{FAR}$ values are associated to a lower shading rate, evidencing that less shadowed buildings are mostly surrounded by low-density areas. The tendency that identifies large-surface buildings being significantly less shaded, is also confirmed by the number of neighbours (N_{neigh}). One could expect that a weaker shading may be related to buildings that have a few neighbours. However, observing le boxplot of N_{neigh} the results show the opposite for this case study. This can be explained by the fact that large-surface buildings are more likely to have more neighbouring constructions compared to tower-like or small constructions.

The average distance with neighbouring constructions ($\bar{d}$) seems not significant to detect the differences between Q_{10} and Q_{90}, as it fails in capturing any information about the size (both in terms of height and area) of the surrounding building. In contrast, as expected, the average height of the building neighbours ($\bar{H}$) shows a small variability and comparatively lower values for less shaded building (Q_{90}).

Finally, as expected, the height difference with surrounding constructions ($\overline{\Delta H}$) is mostly positive for more shaded buildings, i. e. neighbours are higher than the building itself, whereas it is negative or near to zero for the less shaded ones.

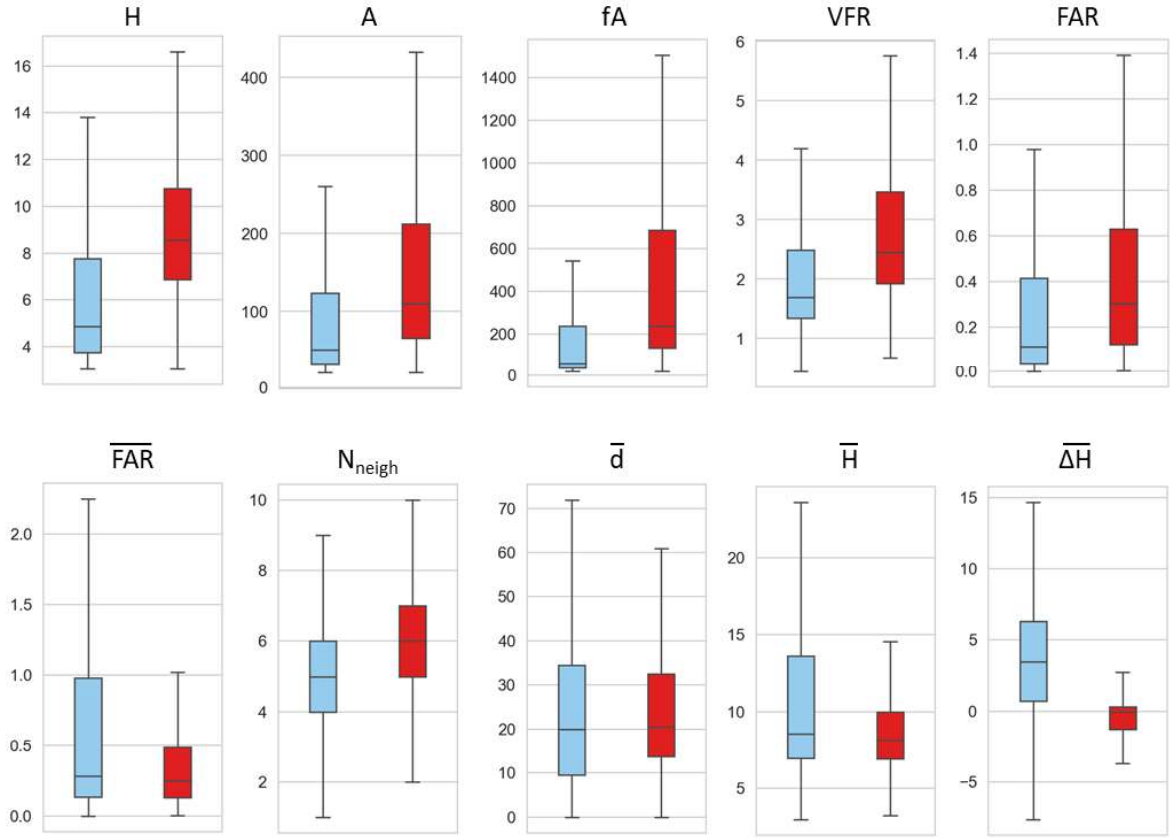

Figure 8: Boxplots of Q_{10} (light blue) and Q_{90} (red). Boxplots show the minimum (lower cap), maximum (upper cap), median (box middle line), 25th percentile (lower box limit), and 75th percentile (upper box limit).

6.3 Correlation study

As briefly outlined in Section 5 a series of data cleaning and pre-processing operations have been performed before investigating the correlations between I* and the morphological features (M_n). Figure 9 shows the detection, through the Isolation Forest method, of the removed outliers for the footprint area values. Each marker represents one building, labelled through its ID number (ranging from 0 to 60,000) on the x-axis and the colours identify the inliers (grey points) and the outliers (red triangles). The same procedure has been applied also for the height and the area of the tessellation cell, the diagrams are not displayed for the sake of conciseness. As a result, a total of about 150 outlier buildings have been removed from the dataset before performing the correlation analysis. The aim of such a pre-treatment operation is to exclude specific buildings with uncommon characteristics in the statistical analysis in order to reduce the induced bias.

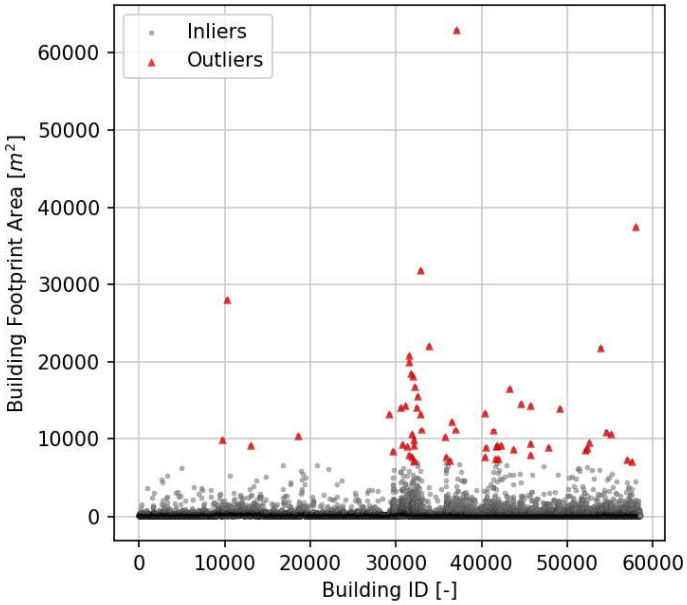

Figure 9: Scatterplot representing the detection of outliers in footprint areas (m^2) in red triangles, and the inliers in grey points

As a preliminary analysis to investigate the relationship between I* and the 40 morphological features (M_n) here considered (see Appendix), the calculation of the Pearson correlation coefficients (R^2) has been performed on the whole dataset. Table 1 shows the R^2 values between I* and each morphological feature of the present study. The results are sorted in descending order of R^2 absolute value with rows and columns. The markers next to the parameter name specify if the R^2 value is the result of a log-log (††) or square root (†) transformation, in case one of the two provided higher correlation coefficients in absolute value compared to the not-transformed data. The parameters related to the height difference between buildings ($\overline{\Delta H}$, $\overline{\Delta H}^+$, α, α^+) and the building rooftop average slope ($\overline{\beta}$) shows moderate (0.39-0.45) correlation coefficients. On the contrary, all the other spatial metrics related to dimension, shape, density, and spatial distribution have very low or no significant correlations with I*. As a general comment, the parameters related to the building shape are the ones that exhibit the worst correlation coefficients at it was expected.

Table 1: Pearson correlation coefficients considering the whole building dataset

$\overline{\Delta H}$	**-0.45**	$\overline{FAR}$	-0.17	Cco (††)	0.09	A_{tess} (††)	0.07
$\overline{\Delta H}^+$ (†)	**-0.43**	P (††)	0.16	FrD (†)	-0.09	$\overline{d}$ (††)	0.06
$\overline{\beta}$	**-0.39**	LaL (††)	0.15	$\overline{fA}$ (††)	-0.09	Ali	-0.06
α^+	-0.25	FAR (††)	0.14	LaL_{tess} (††)	0.09	Sqco	0.05
α	-0.25	Rug (††)	0.14	$\overline{V}$ (††)	-0.08	$\overline{A}$ (††)	-0.04
V (††)	0.21	$\overline{H}$	-0.12	Elo (††)	0.08	Rec	0.04
fA (††)	0.20	$\overline{CAR}$	-0.11	Squ (††)	-0.08	CovA (††)	0.03
VFR (††)	0.20	N_{neigh} (††)	0.11	FoF (††)	-0.08	SWR (††)	0.03
H (††)	0.20	Adj (††)	0.11	CAR (††)	0.08	$\overline{A_{tess}}$ (†)	-0.01
A (††)	0.18	ShIdx (††)	0.09	HW (††)	0.07	ERI	0.01

(†) Square root transformation
(††) Log-log transformation

Despite the low correlation values, observing the scatterplots representing the relationship between I* and the morphological parameters, in some cases a "triangular" pattern can be noticed. More precisely,

for the parameters related to the building dimension (namely A, H, V, P, fA, VFR, LaL), called $M_{n,dim}$ for brevity, it is possible to define a relationship of the type $I^* > a \cdot M_{n,dim} + b$ (or $\log(I^*) > a \cdot \log(M_{n,dim}) + b$ in case of log-log transformation) through a quantile regression. Figure 10 shows the scatterplot between I* (y-axis) and V (x-axis) after the log-log transformation. As it can be noticed, the variability of log(I*) is so high for lower log(V) values, that the linear correlation between the two, represented by the black regression line, is unsuitable to describe the data. On the other hand, performing a quantile linear regression by considering the 0.01 quantiles of data (red points) it is possible to define a regression line (red line) with R^2=0.87. Despite it is not possible to predict I* based on $M_{n,dim}$, using a quantile linear regression it is possible to define the most probable range of I* values corresponding to a selected $M_{n,dim}$ value. Worth noting that the same considerations presented for V apply to the other dimensional features of the building (A, H, P, fA, VFR, LaL).

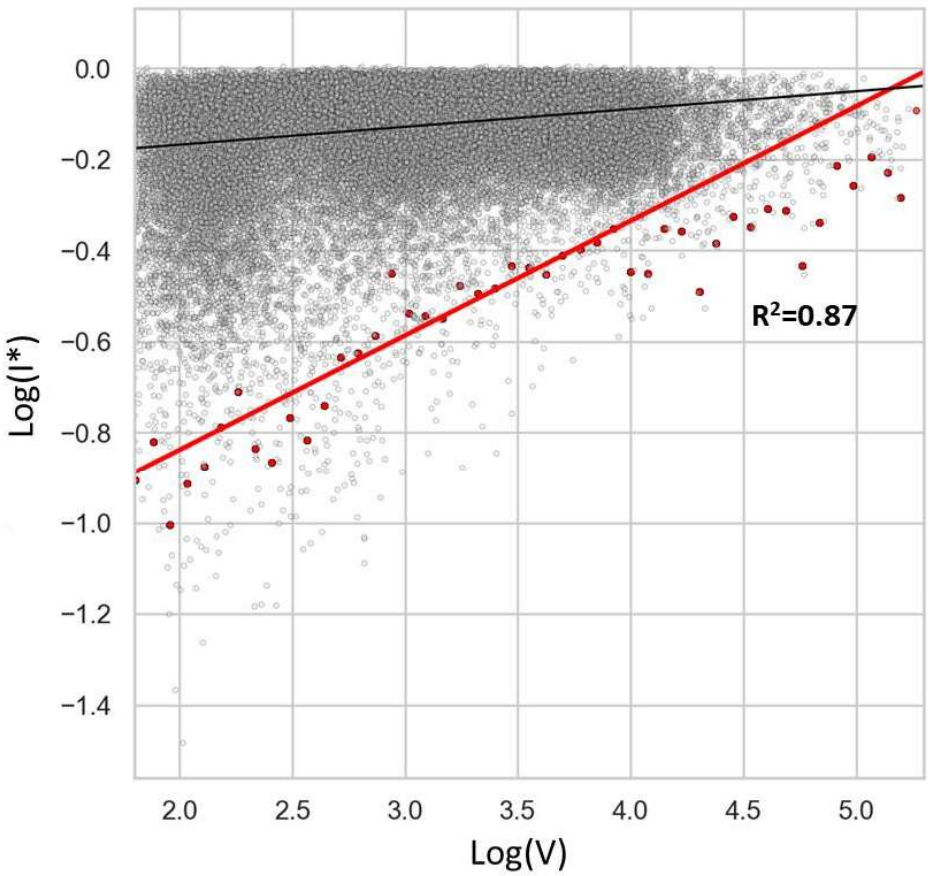

Figure 10: Scatterplot between log(I) and log(V). The black line represents the linear regression line and the red line is related to the linear quantile regression line based on 0.01 quantiles (red points).*

6.4 Correlation analysis by municipality

The Canton of Geneva is a rather heterogeneous territory, composed of 48 municipalities, some being small rural municipalities, others being part of the urban area of the Geneva city itself. By analysing the average morphological features characterising each of the 48 municipalities of the Canton of Geneva, some evident differences can be noticed. In particular, four out of the 48 municipalities appear overscale both in terms of building size and of built density. The four municipalities correspond to the city centre district, having a denser urban morphology compared to the more open residential suburbs. Figure 11 shows the boxplots related to the building volume (V) and the building Floor Area Ratio (FAR) for each municipality, evidencing in red the four municipalities that correspond to the Geneva city centre.

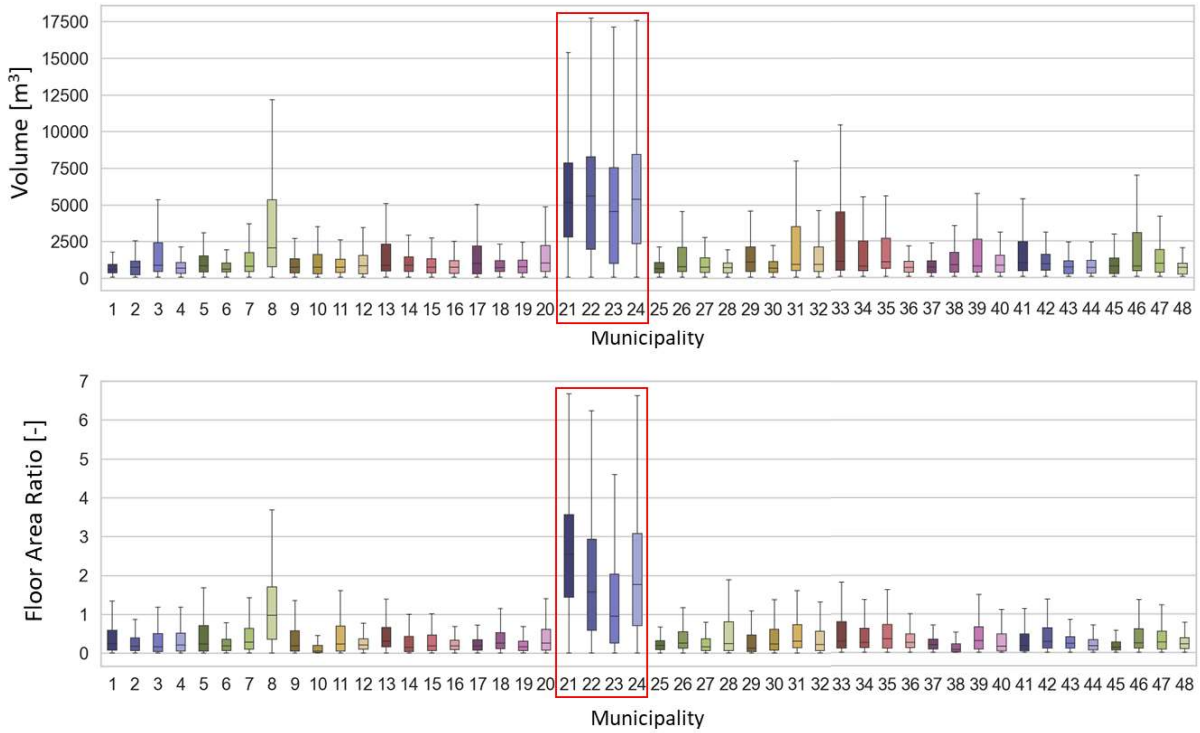

Figure 11: Boxplots of V and FAR of the 48 municipalities of the Canton of Geneva. The city centre districts are highlighted with red boxes.

The linear Pearson correlation coefficients have been calculated considering a reduced dataset of buildings, including only the four city centre municipalities. The results are reported in Table 2. As it can be observed, in this case, the correlations between I* and the morphological parameters are higher. As in the previous case, the most relevant parameters to describe I* are the ones related to the height difference with surrounding buildings (R^2 about 0.6). Additionally, also some building dimension features (namely H, fA, V, FoF, VFR, A) show moderate correlation coefficients towards I* (0.32-0.53).

Table 2: Pearson correlation coefficients considering the 4 city centre districts

$\overline{\Delta H}$ (†)	**-0.60**	A_{tess} (††)	0.29	ShIdx (†)	0.22	$\overline{H}$ (†)	0.12
$\overline{\Delta H}^{+}$ (†)	**-0.58**	LaL_{tess} (††)	0.28	FrD (††)	-0.21	$\overline{FAR}$	0.11
H (††)	**0.53**	$\overline{d}$ (††)	0.27	Elo (††)	0.20	Rec	0.09
fA (††)	**0.47**	FAR (††)	0.27	HW (†)	0.20	Squ (††)	-0.09
V (††)	**0.47**	P (††)	0.26	CovA (††)	0.20	$\overline{A}$ (††)	0.08
FoF (††)	**-0.38**	Adj (††)	0.25	$\overline{A_{tess}}$ (††)	0.17	$\overline{V}$ (††)	0.07
VFR (††)	**0.35**	Rug (††)	0.25	$\overline{CAR}$	0.17	$\overline{fA}$ (††)	0.07
α	**-0.32**	$\overline{\beta}$	-0.25	CAR	0.15	ERI	0.03
A (††)	**0.32**	LaL (††)	0.24	Sqco (†)	0.15	SWR (†)	0.03
α^{+}	**-0.31**	Cco (†)	0.23	N_{neigh} (††)	0.12	Ali (†)	0.02

(†) Square root transformation
(††) Log-log transformation

The most meaningful correlation is shown in Figure 12, representing the scatterplot between I* and the building average height difference with surrounding ($\overline{\Delta H}$), after the square root transformation, as well as the regression line with the related equation. In general, the greater is the height difference with the

surroundings, the lower is the I* value, meaning that the buildings are more likely to be shaded by the neighbouring constructions.

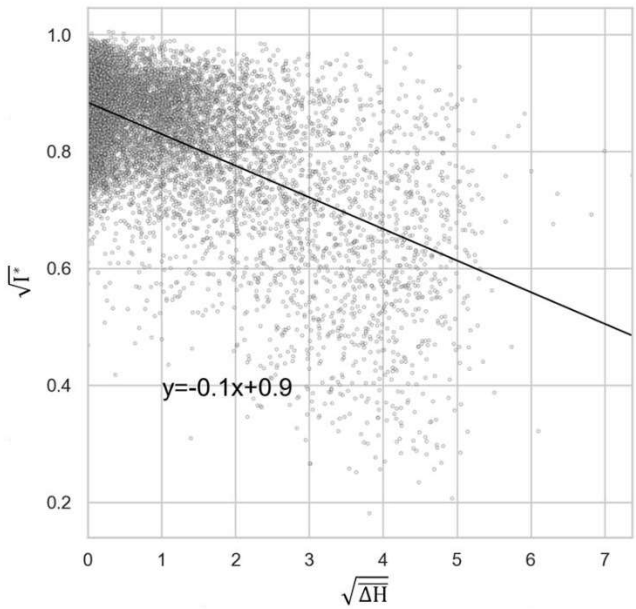

Figure 12: Scatterplot between I and $\overline{\Delta H}$ after the square root transformation. The black line represents the linear regression line.*

The results arising from this correlation study evidence that some tendencies and meaningful information about rooftop shading conditions, and more in general on solar radiation analyses, can be extracted through detailed urban morphological studies. However, for most of the selected parameters the correlation coefficients are not sufficient to suggest accurate predictive models. The features related to the building dimension and the height difference with the surrounding constructions are the most useful to investigate the overall rooftop shading rate and they provide interesting qualitative considerations both for researchers and planners. Contrarily to solar radiation on façades [19–21], the analysed density-related parameters do not show meaningful relationship towards solar radiation conditions. On the other hand, as it has been presented for the four downtown municipalities, the density is a meaningful measure of the impact level of urban morphology on shading conditions. The higher is the built density, the grater is the effect of surrounding constructions of rooftop solar radiation.

7 Conclusions and perspectives

In this paper we propose a new general methodology to investigate the relationship between rooftop insolation and urban morphology. A comprehensive statistical analysis has been performed with respect to rooftop solar producibility related to the Canton of Geneva, Switzerland. About 60 thousand buildings have been considered for a detailed analysis based on 40 urban morphological parameters. The selected morphological features refer to building dimension, shape, interbuilding geometrical parameters as differences in height, distance, land area occupancy whose values have been calculated thanks to a Python Authors' code able to process GIS-data.

The independent variables (the urban morphological parameters) have been statistically processed versus the dimensionless insolation, defined in the present study as the ratio of the Solar Cadaster previously calculated insolation values and the unshaded insolation per roof portion.

In the present studies it is showed that:

- Within the studied area, more than 75% of the buildings is partly shaded. On the other hand, 75% of the buildings receive more than 69 % of the solar insolation that they would receive if they were not shaded.

- The most shaded buildings (0.1 quantile) and least shaded (0.9 quantile) feature significantly different morphological characteristics. The least shaded ones are more likely to be low-rise large buildings (with big surfaces) rather than high-rise/tower-like constructions, as it could be expected.
- At the scale of the Canton of Geneva, correlations between the scaled irradiance and the morphological are rather low, reaching a maximum R^2 of 0.45 for $\overline{\Delta H}$. However, analysing the municipalities, correlations are significantly improved for dense urban patterns (city centre), with R^2 coefficient that can reach up to 0.60.
- In general, the morphological parameters that exhibit the best correlations are the ones related to building dimension and interbuilding height difference, in particular referring to the city centre municipalities. On the contrary, the features related to density and building shape have low or irrelevant correlation coefficients.
- In some cases, according to the heterogeneity of the large dataset, correlation coefficient may not appear as the most relevant indicator. Instead, a correlation of the lowest quantiles can appear to well represent the dataset with correlation coefficient by up to 0.87.

In order to pursue the proposed approach, it would be interesting to apply it to other territories with different weather, latitude as well as urban morphology. However, this requires the access to large data set of rooftop irradiance, which unfortunately is not common to find in open-access.

As mentioned earlier, it is also worth mentioning that the proposed methodology can be applied to any type of urban surface, including vertical façades. The latter would be extremely interesting since these surfaces are more likely to be sensitive to shadings from surroundings.

Finally, the proposed approach is not limited to solar analysis. Indeed, it can be applied to any type of variable related to the urban microclimate such as, for example pollution, or temperature.

Acknowledgements

This research has been supported by the program MITI (Mission for Transversal and Interdisciplinary Initiatives) of CNRS and CSTB through the CITYBIOM project, and by the French National Research Agency, through the Investments for Future Program (ref. ANR-18-EURE-0016 - Solar Academy). The research unit LOCIE is a member of the INES Solar Academy Research Center. Authors would like to thanks Gilles Desthieux and the program INTERREG V Suisse-France for providing data about solar irradiance in the Greater Geneva territory.

8 Appendix

Name	Description	Cat	Symbol	Equation	Unit
Building height	Building height	D	H	-	[m]
Building area	Building footprint area	D	A	-	[m^2]
Building total floor area	Total floor area of the building, i.e. footprint area multiplied by the number of floors (n° floors)	D	fA	$fA = A \cdot n°floors$	[m^2]
Building volume	Building volume	D	V	$V = A \cdot H$	[m^3]
Building perimeter	Sum of lengths of the building exterior walls	D	P	-	[m]
Building longest axis length	Diameter of the minimal circumscribed circle around the building footprint	D	LaL	-	[m]
Building volume to façade ratio	Ratio between building volume and the total area of façades	D	VFR	$VFR = \frac{V}{P \cdot H}$	[m^3/m^2]
Building fractal dimension	Statistical index of the complexity of a geometry	D	FrD	$FrD = \frac{2\log(P/2)}{\log(A)}$	
Building form factor	Quantity representing the 3D unitless shape characteristics of a building envelope unbiased by the building size	D	FoF	$FoF = \frac{A}{(V)^{2/3}}$	[-]
Tessellation area	Area of the tessellation cell	D	A_{tess}	-	[m^2]
Tessellation longest axis length	Diameter of the minimal circumscribed circle around the tessellation cell	D	LaL_{tess}	-	[m]

Building circular compactness	Index of the similarity of a shape with a circle. It is based on the area of the minimal enclosing circle (A_c)	S	Cco	$Cco = \frac{A}{A_c}$	[-]
Building square compactness	Measure of the compactness of the building footprint	S	Sqco	$Sqco = \left(\frac{4\sqrt{A}}{P}\right)^2$	[-]
Building squareness	Mean deviation μ of each i corner of the building from 90 degrees. N_{cor} is the number of corners	S	Squ	$Squ = \frac{\sum_{i=1}^{N_{cor}} \mu_i}{N_{cor}}$	[-]
Building Rectangularity	Index of the similarity of a shape with a rectangle. It is based on the area of the minimal rotated bounding rectangle of the building (A_{MBR})	S	Rec	$Rec = \frac{A}{A_{MBR}}$	[-]
Building shape index	Shape index of the building footprint	S	ShIdx	$ShIdx = \frac{\sqrt{\frac{A}{\pi}}}{0.5 \cdot LaL}$	[-]
Building equivalent rectangular index	Measure of shape complexity based on the area of the minimal rotated bounding rectangle of a building (A_{MBR}) and its perimeter (P_{MBR})	S	ERI	$ERI = \sqrt{\frac{A}{A_{MBR}}} \cdot \frac{P_{MBR}}{P}$	[-]
Building elongation	Measure of the deviation of the building shape from a square based on the length of the minimal rotated bounding rectangle of a building (L_{MBR}) and its width (l_{MBR})	S	Elo	$Elo = \frac{L_{MBR}}{l_{MBR}}$	[-]
Coverage area ratio	Ratio between the building footprint area and the area of the related tessellation cell	I	CAR	$CAR = \frac{A}{A_{tess}}$	[-]
Floor area ratio	Ratio between the building total floor area and the area of the related tessellation cell	I	FAR	$FAR = \frac{fA}{A_{tess}}$	[-]

Rugosity	Ratio between the building volume and the area of the related tessellation cell	I	Rug	$Rug = \frac{V}{A_{tess}}$	[m^3/m^2]
Shared walls ratio of adjacent buildings	Ratio between the length of the perimeter shared with adjacent buildings (P_{shared}) and the building perimeter	SD	SWR	$SWR = \frac{P_{shared}}{P}$	[-]
Number of neighbours	Number of neighbouring buildings	SD	N_{neigh}	-	[-]
Alignment	Mean deviation of solar orientation (dev_{sol}) of neighbouring buildings	SD	Ali	$Ali = \frac{1}{N_{neigh}} \sum_{j \in neigh} dev_{sol}(j)$	[-]
Building adjacency	Ratio between the number of joined adjacent structures ($N_{neigh,join}$) and the number of neighbouring buildings (N_{neigh})	SD	Adj	$Adj = \frac{N_{neigh,join}}{N_{neigh}}$	[-]
Mean inter-building distance	Mean distance between the building and the adjacent buildings	SD	$\bar{d}$	$\bar{d} = \frac{1}{N_{neigh}} \sum_{j \in neigh} d(j)$	[m]
Mean coverage area ratio	Mean coverage area ratio of the neighbouring tessellation cells	SD	$\overline{CAR}$	$\overline{CAR} = \frac{1}{N_{neigh}} \sum_{j \in neigh} CAR(j)$	[-]
Mean floor area ratio	Mean floor area ratio of the neighbouring tessellation cells	SD	$\overline{FAR}$	$\overline{FAR} = \frac{1}{N_{neigh}} \sum_{j \in neigh} FAR(j)$	[-]
Covered area	Total area covered by the building itself and its neighbours	SD	CovA	$CovA = A + \sum_{j \in neigh} A(j)$	[m^2]
Average building area	Mean footprint area of building neighbouring constructions	SD	$\bar{A}$	$\bar{A} = \frac{1}{N_{neigh}} \sum_{j \in neigh} A(j)$	[m^2]
Average building height	Mean height of building neighbouring constructions	SD	$\bar{H}$	$\bar{H} = \frac{1}{N_{neigh}} \sum_{j \in neigh} H(j)$	[m]

Average building volume	Mean height of building neighbouring constructions	SD	$\overline{V}$	$\overline{V} = \frac{1}{N_{neigh}} \sum_{j \in neigh} V(j)$	[m^3]
Average building total floor area	Mean total floor area of building neighbouring constructions	SD	$\overline{fA}$	$\overline{fA} = \frac{1}{N_{neigh}} \sum_{j \in neigh} fA(j)$	[m^2]
Average tessellation area	Mean tessellation area of building neighbouring tessellation cells	SD	$\overline{A_{tess}}$	$\overline{A_{tess}} = \frac{1}{N_{neigh}} \sum_{j \in neigh} A_{tess}(j)$	[m^2]
D=dimension S=shape I=intensity SD=spatial distribution					

References

[1] European Commission, Energy performance of buildings directive revision, (2018) 17–18. https://ec.europa.eu/energy/en/news/commission-%0Awelcomes- agreement- energy-performance- buildings %0A (accessed November 23, 2021).

[2] B. Güneralp, Y. Zhou, D. Ürge-Vorsatz, M. Gupta, S. Yu, P.L. Patel, M. Fragkias, X. Li, K.C. Seto, Global scenarios of urban density and its impacts on building energy use through 2050, Proc. Natl. Acad. Sci. U. S. A. 114 (2017) 8945–8950. https://doi.org/10.1073/pnas.1606035114.

[3] J. Brozovsky, A. Gustavsen, N. Gaitani, Zero emission neighbourhoods and positive energy districts – A state-of-the-art review, Sustain. Cities Soc. 72 (2021) 103013. https://doi.org/10.1016/J.SCS.2021.103013.

[4] A. Boccalatte, M. Fossa, C. Ménézo, Best arrangement of BIPV surfaces for future NZEB districts while considering urban heat island effects and the reduction of reflected radiation from solar façades, Renew. Energy. 160 (2020) 686–697. https://doi.org/10.1016/j.renene.2020.07.057.

[5] IEA, Technology Roadmap - Solar Photovoltaic Energy 2014, 2014. https://www.iea.org/reports/technology-roadmap-solar-photovoltaic-energy-2014.

[6] S. Freitas, C. Catita, P. Redweik, M.C. Brito, Modelling solar potential in the urban environment: State-of-the-art review, Renew. Sustain. Energy Rev. 41 (2015) 915–931. https://doi.org/10.1016/j.rser.2014.08.060.

[7] J. Kanters, M. Wall, E. Kjellsson, The Solar Map as a Knowledge Base for Solar Energy Use, Energy Procedia. 48 (2014) 1597–1606. https://doi.org/10.1016/J.EGYPRO.2014.02.180.

[8] G. Lobaccaro, M.M. Lisowska, E. Saretta, P. Bonomo, F. Frontini, A Methodological Analysis Approach to Assess Solar Energy Potential at the Neighborhood Scale, Energies 2019, Vol. 12, Page 3554. 12 (2019) 3554. https://doi.org/10.3390/EN12183554.

[9] H.C. Chen, Q. Han, B. de Vries, Urban morphology indicator analyzes for urban energy modeling, Sustain. Cities Soc. 52 (2020). https://doi.org/10.1016/j.scs.2019.101863.

[10] T. Martins, L. Adolphe, M. Bonhomme, Building Energy Demand Based on Urban Morphology Case Study in Maceió , Brazil, PLEA 2013 Sustain. Archit. a Renew. Futur. (2013) 1–6. http://mediatum.ub.tum.de/doc/1169253/1169253.pdf.

[11] G. Tardioli, A. Narayan, R. Kerrigan, M. Oates, J. O'Donnell, D.P. Finn, A methodology for calibration of building energy models at district scale using clustering and surrogate techniques, Energy Build. 226 (2020) 110309. https://doi.org/10.1016/j.enbuild.2020.110309.

[12] Z. Shi, J.A. Fonseca, A. Schlueter, A parametric method using vernacular urban block typologies for investigating interactions between solar energy use and urban design, Renew. Energy. 165 (2021) 823–841. https://doi.org/10.1016/j.renene.2020.10.067.

[13] D. Robinson, Urban morphology and indicators of radiation availability, Sol. Energy. 80 (2006) 1643–1648. https://doi.org/10.1016/j.solener.2006.01.007.

[14] J.J. Sarralde, D.J. Quinn, D. Wiesmann, K. Steemers, Solar energy and urban morphology: Scenarios for increasing the renewable energy potential of neighbourhoods in London, Renew. Energy. 73 (2015) 10–17. https://doi.org/10.1016/J.RENENE.2014.06.028.

[15] C. Carneiro, E. Morello, G. Desthieux, F. Golay, Urban environment quality indicators: application to solar radiation and morphological analysis on built area, Adv. Vis. Imaging Simul. (2010).

[16] J. Scartezzini, R. Compagnon, Comparison of the solar energy utilisation potential of different urban environments, Proc. PLEA. (2004). https://www.academia.edu/14733584/Comparison_of_the_solar_energy_utilisation_potential_of_different_urban_environments (accessed November 25, 2021).

[17] N. Mohajeri, A. Gudmundsson, T. Kunckler, G. Upadhyay, D. Assouline, J.H. Kämpf, J.L. Scartezzini, A solar-based sustainable urban design: The effects of city-scale street-canyon geometry on solar access in Geneva, Switzerland, Appl. Energy. 240 (2019) 173–190.

https://doi.org/10.1016/j.apenergy.2019.02.014.
[18] K.H. Poon, J.H. Kämpf, S.E.R. Tay, N.H. Wong, T.G. Reindl, Parametric study of URBAN morphology on building solar energy potential in Singapore context, Urban Clim. 33 (2020) 100624. https://doi.org/10.1016/j.uclim.2020.100624.
[19] C. Chatzipoulka, R. Compagnon, M. Nikolopoulou, Urban geometry and solar availability on façades and ground of real urban forms: using London as a case study, Sol. Energy. 138 (2016) 53–66. https://doi.org/10.1016/j.solener.2016.09.005.
[20] N. Mohajeri, G. Upadhyay, A. Gudmundsson, D. Assouline, J. Kämpf, J.L. Scartezzini, Effects of urban compactness on solar energy potential, Renew. Energy. 93 (2016) 469–482. https://doi.org/10.1016/j.renene.2016.02.053.
[21] M. Morganti, A. Salvati, H. Coch, C. Cecere, Urban morphology indicators for solar energy analysis, Energy Procedia. 134 (2017) 807–814. https://doi.org/10.1016/j.egypro.2017.09.533.
[22] J. Dibble, A. Prelorendjos, O. Romice, M. Zanella, E. Strano, M. Pagel, S. Porta, On the origin of spaces: Morphometric foundations of urban form evolution:, EPB Urban Anal. City Sci. 46 (2017) 707–730. https://doi.org/10.1177/2399808317725075.
[23] G. Boeing, Off the Grid…and Back Again?, J. Am. Plan. Assoc. 87 (2020) 123–137. https://doi.org/10.1080/01944363.2020.1819382.
[24] A. Araldi, G. Fusco, From the street to the metropolitan region: Pedestrian perspective in urban fabric analysis:, EPB Urban Anal. City Sci. 46 (2019) 1243–1263. https://doi.org/10.1177/2399808319832612.
[25] M. Fleischmann, A Systematisation of Attributes for Quantitative Urban Morphology Measuring Urban Form, (2017).
[26] M. Fleischmann, Methodological Foundation of a Numerical Taxonomy of Urban Form, (n.d.) 1–86.
[27] M. Fleischmann, A. Feliciotti, W. Kerr, Evolution of Urban Patterns: Urban Morphology as an Open Reproducible Data Science, Geogr. Anal. (2021) 1–23. https://doi.org/10.1111/gean.12302.
[28] M. Fleischmann, A. Feliciotti, O. Romice, S. Porta, Morphological tessellation as a way of partitioning space: Improving consistency in urban morphology at the plot scale, Comput. Environ. Urban Syst. 80 (2020) 101441. https://doi.org/10.1016/j.compenvurbsys.2019.101441.
[29] M. Fleischmann, momepy: Urban Morphology Measuring Toolkit, J. Open Source Softw. 4 (2019) 1807. https://doi.org/10.21105/JOSS.01807.
[30] G. Desthieux, C. Carneiro, A. Susini, N. Abdennadher, A. Boulmier, A. Dubois, R. Camponovo, D. Beni, M. Bach, P. Leverington, E. Morello, Solar Cadaster of Geneva: A Decision Support System for Sustainable Energy Management, From Sci. to Soc. (2018) 129–137. https://doi.org/10.1007/978-3-319-65687-8_12.
[31] G. Desthieux, C. Carneiro, R. Camponovo, P. Ineichen, E. Morello, A. Boulmier, N. Abdennadher, S. Dervey, C. Ellert, Solar energy potential assessment on rooftops and facades in large built environments based on lidar data, image processing, and cloud computing. Methodological background, application, and validation in geneva (solar cadaster), Front. Built Environ. 4 (2018). https://doi.org/10.3389/fbuil.2018.00014.
[32] SITG | Le territoire genevois à la carte, (n.d.). https://ge.ch/sitg/ (accessed November 29, 2021).
[33] M. Thebault, V. Clivillé, L. Berrah, G. Desthieux, Multicriteria roof sorting for the integration of photovoltaic systems in urban environments, Sustain. Cities Soc. 60 (2020) 102259. https://doi.org/10.1016/j.scs.2020.102259.
[34] J.E. Hay, Calculation of monthly mean solar radiation for horizontal and inclined surfaces, Sol. Energy. 23 (1979) 301–307. https://doi.org/10.1016/0038-092X(79)90123-3.
[35] C. Ratti, P. Richens, Raster Analysis of Urban Form:, Environ. Plan. B Urban Anal. City Sci. 31 (2016) 297–309. https://doi.org/10.1068/B2665.
[36] K. Jordahl, J. Van den Bossche, J. Wasserman, J. McBride, J. Gerard, M. Fleischmann, J. Tratner, M. Perry, C. Farmer, G.A. Hjelle, S. Gillies, M. Cochran, M. Bartos, L. Culbertson, N.

Eubank, maxalbert, S. Rey, A. Bilogur, D. Arribas-Bel, C. Ren, J. Wilson, M. Journois, L.J. Wolf, L. Wasser, Ö. Özak, YuichiNotoya, F. Leblanc, Filipe, C. Holdgraf, A. Greenhall, geopandas/geopandas: v0.6.1, (2019). https://doi.org/10.5281/ZENODO.3483425.

[37] S.J. Rey, L. Anselin, PySAL: A Python Library of Spatial Analytical Methods, Rev. Reg. Stud. 37 (2010) 175–193. https://doi.org/10.1007/978-3-642-03647-7_11.

[38] A.A. Hagberg, D.A. Schult, P.J. Swart, Proceedings of the Python in Science Conference (SciPy): Exploring Network Structure, Dynamics, and Function using NetworkX, in: Proc. 7th Python Sci. Conf., Pasadena, CA USA, 2008: pp. 11–15. http://conference.scipy.org/proceedings/SciPy2008/paper_2/.

[39] L. Buitinck, G. Louppe, M. Blondel, F. Pedregosa, A.C. Müller, O. Grisel, V. Niculae, P. Prettenhofer, A. Gramfort, J. Grobler, R. Layton, J. Vanderplas, A. Joly, B. Holt, G. Varoquaux, API design for machine learning software: experiences from the scikit-learn project, (2013). https://arxiv.org/abs/1309.0238v1 (accessed December 1, 2021).

[40] J.P. Stevens, Applied Multivariate Statistics for the Social Sciences, 5th ed., John Wiley & Sons, Ltd, 2002. https://doi.org/10.1111/J.1751-5823.2009.00095_13.X.